

1 **Revision 1**

2

3 **Seaborgite, $\text{LiNa}_6\text{K}_2(\text{UO}_2)(\text{SO}_4)_5(\text{SO}_3\text{OH})(\text{H}_2\text{O})$, the first uranyl mineral containing**
4 **lithium**

5

6 **ANTHONY R. KAMPF^{1§}, TRAVIS A. OLDS², JAKUB PLÁŠIL³, JOE MARTY⁴, SAMUEL N. PERRY⁵,**
7 **LORETTA CORCORAN⁵ AND PETER C. BURNS^{5,6}**

8

9 ¹ Mineral Sciences Department, Natural History Museum of Los Angeles County, 900 Exposition Boulevard, Los
10 Angeles, CA 90007, USA

11 ² Section of Minerals and Earth Sciences, Carnegie Museum of Natural History, 4400 Forbes Avenue, Pittsburgh,
12 Pennsylvania 15213, USA

13 ³ Institute of Physics ASCR, v.v.i., Na Slovance 1999/2, 18221 Prague 8, Czech Republic

14 ⁴ 5199 East Silver Oak Road, Salt Lake City, UT 84108, USA

15 ⁵ Department of Civil and Environmental Engineering and Earth Sciences, University of Notre Dame, Notre Dame,
16 IN 46556, USA

17 ⁶ Department of Chemistry and Biochemistry, University of Notre Dame, Notre Dame, IN 46556, USA

18

19 **ABSTRACT**

20 Seaborgite (IMA2019-087), $\text{LiNa}_6\text{K}_2(\text{UO}_2)(\text{SO}_4)_5(\text{SO}_3\text{OH})(\text{H}_2\text{O})$, is a new mineral species from
21 the Blue Lizard mine, Red Canyon, San Juan County, Utah, U.S.A. It is a secondary phase found
22 on gypsum in association with copiapite, ferrinatrite, ivsite, metavoltine, and römerite. Seaborgite
23 occurs in sprays of light-yellow, long flattened prisms or blades, up to about 0.2 mm in length.

[§] Email: akampf@nhm.org

24 Crystals are elongated on [100], flattened on {010}, and exhibit the forms {100}, {010}, {001},
25 and {10-1}. The mineral is transparent with vitreous luster and very pale-yellow streak. It
26 exhibits bright lime-green fluorescence under a 405 nm laser. The Mohs hardness is $\sim 2\frac{1}{2}$. The
27 mineral has brittle tenacity, curved or conchoidal fracture, and one good cleavage on {100}. The
28 measured density is $2.97(2) \text{ g}\cdot\text{cm}^{-3}$. The mineral is immediately soluble in RT H₂O. The mineral
29 is optically biaxial (-), $\alpha = 1.505(2)$, $\beta = 1.522(2)$, $\gamma = 1.536(2)$ (white light); $2V_{\text{meas}} = 85(1)^\circ$;
30 moderate $r < v$ dispersion; orientation $X \wedge \mathbf{a} \approx 10^\circ$; pleochroic X colourless, Y and Z light green-
31 yellow; $X < Y \approx Z$. Seaborgite EPMA and LA-ICP-MS analyses undermeasured Li, K, and Na.
32 The empirical formula using Li, Na, and K based on the structure refinement is
33 $\text{Li}_{1.00}\text{Na}_{5.81}\text{K}_{2.19}(\text{UO}_2)(\text{SO}_4)_5(\text{SO}_3\text{OH})(\text{H}_2\text{O})$. Seaborgite is triclinic, $P-1$, $a = 5.4511(4)$, $b =$
34 $14.4870(12)$, $c = 15.8735(15) \text{ \AA}$, $\alpha = 76.295(5)$, $\beta = 81.439(6)$, $\gamma = 85.511(6)^\circ$, $V = 1203.07(18)$
35 \AA^3 , and $Z = 2$. The structure ($R_1 = 0.0377$ for $1935 I > 2\sigma I$) contains $[(\text{UO}_2)_2(\text{SO}_4)_8]^{4-}$ uranyl-
36 sulfate clusters that are linked into a band by bridging LiO_4 tetrahedra. The bands are linked
37 through peripheral SO_4 tetrahedra forming a thick heteropolyhedral layer. Channels within the
38 layers contain a K site, while an additional K site, six Na sites, and an SO_3OH group occupy the
39 space between the heteropolyhedral layers.

40
41 *Keywords:* seaborgite; new mineral species; lithium; uranyl sulfate; crystal structure; Blue Lizard
42 mine, Red Canyon, Utah.

43

44

INTRODUCTION

45 The Blue Lizard mine in Red Canyon, Utah is a remarkable source of new minerals,
46 especially sodium-uranyl sulfates. The astounding diversity and relatively high structural

47 complexity of uranyl-sulfate minerals was recently emphasized by Gurzhiy and Plášil (2019). A
48 large number of stable combinatorial linkages of uranyl and sulfate tetrahedra are possible, with
49 the topological arrangements appearing to be strongly affected by at least three parameters: pH
50 (Plášil et al. 2014), cation content, and water content. In general, sodium-uranyl-sulfate minerals
51 follow the same structural unit topology trends as do other uranyl minerals (Lussier et al. 2016),
52 where uranyl polyhedra preferentially polymerize into extended structures *via* linkages through
53 their equatorial vertices, most often forming infinite chain or infinite sheet topologies. However,
54 finite cluster topologies are relatively abundant among the sodium-uranyl-sulfate minerals, for
55 reasons that are not completely clear. Understanding the hierarchical arrangements of these
56 structures and how conditions of formation influence the crystallized topologies is important to
57 understanding the crystal-chemical nature of U-S systems, and for uranyl mineralogy as a whole.

58 The new Blue-Lizard-mine uranyl sulfate seaborgite, described herein, contains essential
59 sodium; however, it also includes essential potassium and, most significantly, lithium. While
60 sodium and, especially potassium, form relatively weak bonds within such structures, the role of
61 lithium is rather different. Lithium-oxygen bonds, particularly in LiO_4 tetrahedral coordination,
62 are somewhat stronger and, in the seaborgite structure, serve to further link (or polymerize) the
63 uranyl sulfate clusters.

64 Seaborgite is named in honor of American chemist Glenn T. Seaborg (1912–1999) who
65 was involved in the synthesis, discovery, and investigation of 10 transuranium elements
66 (including seaborgium), earning him a share of the 1951 Nobel Prize in Chemistry. Seaborg's
67 scientific accomplishments are numerous and changed the course of world history. Perhaps most
68 notably, Seaborg and coworkers discovered plutonium in 1940 and he isolated the first weighable
69 sample of plutonium in 1942. The Manhattan Project produced the first plutonium-fueled nuclear

70 bomb that was detonated in New Mexico at the Trinity test site on July 16, 1945. Seaborg served
71 as Chairman of the United States Atomic Energy Commission from 1961 to 1971 during which
72 time he worked to advance nuclear energy. Seaborg was a strong proponent for arms control and
73 the peaceful use of nuclear energy.

74 The new mineral and name were approved by the Commission on New Minerals,
75 Nomenclature and Classification of the International Mineralogical Association (IMA 2019-087).
76 One holotype specimen of seaborgite is deposited in the collections of the Natural History
77 Museum of Los Angeles County, Los Angeles, California, USA, catalogue number 74163.

78

79

OCCURRENCE

80 Seaborgite was found underground in the Blue Lizard mine (37°33'26"N 110°17'44"W),
81 Red Canyon, White Canyon District, San Juan County, Utah, USA. The mine is about 72 km
82 west of the town of Blanding, Utah, and about 22 km southeast of Good Hope Bay on Lake
83 Powell. Detailed historical and geologic information on the Blue Lizard mine is described
84 elsewhere (cf. Kampf et al. 2015), and is primarily derived from a report by Chenoweth (1993).

85 Abundant secondary uranium mineralization in Red Canyon is associated with post-
86 mining oxidation of asphaltum-rich sandstone beds laced with uraninite and sulfides in the damp
87 underground environment. Seaborgite was found in an area rich in K-bearing sulfates (e.g.
88 metavoltine, voltaite, zincovoltate), along with several other potentially new sodium and
89 potassium uranyl sulfate minerals. Potassium enrichment has so far not been observed in
90 secondary uranyl mineralization elsewhere in the Blue Lizard mine nor in any of the nearby U
91 deposits in Red Canyon that we have investigated and this is the first uranyl mineral found that
92 contains essential Li. It seems likely that K and Li are sourced from Li- and K-bearing clays in

93 the sediments.

94 Seaborgite is a very rare mineral in the secondary mineral assemblages of the Blue Lizard
95 mine. It occurs on a thick crust of gypsum overlaying matrix comprised mostly of subhedral to
96 euhedral, equant quartz crystals that are recrystallized counterparts of the original grains of the
97 sandstone. Other secondary phases found in close association with seaborgite are copiapite,
98 ferrinatrite, ivsite, metavoltine, römerite, and other potentially new uranyl sulfate minerals.

99

100 PHYSICAL AND OPTICAL PROPERTIES

101 Crystals of seaborgite are long flattened prisms or blades, up to about 0.2 mm in length,
102 typically in radiating sprays (Fig. 1). Crystals are elongated on [100], flattened on {010}, and
103 exhibit the forms {100}, {010}, {001}, and {10-1} (Fig. 2). Twinning was observed optically
104 under crossed polars, and is either by reflection on {001} or by rotation around [001].

105 The mineral is light yellow and transparent with vitreous luster and very pale-yellow
106 streak. Seaborgite exhibits bright lime-green fluorescence under a 405 nm laser. It has a Mohs
107 hardness of about 2½ based on scratch tests. The mineral has brittle tenacity, curved or
108 conchoidal fracture, and one good cleavage on {100}. The density measured by flotation in a
109 mixture of methylene iodide and toluene is 2.97(2) g·cm⁻³. The calculated density is 3.015 g·cm⁻³
110 for the empirical formula (using Li, Na, and K based on the structure refinement) and single-
111 crystal cell; 3.004 g·cm⁻³ for the ideal formula. The mineral is immediately soluble in H₂O at
112 room temperature.

113 Seaborgite is optically biaxial (-) with $\alpha = 1.505(2)$, $\beta = 1.522(2)$, $\gamma = 1.536(2)$ measured
114 in white light. The 2V measured using extinction data analyzed with EXCALIBRW (Gunter et al.
115 2004) is 85(1)°; the calculated 2V is 83.6°. The dispersion is moderate, $r < v$. The partially

116 determined optical orientation is $X \wedge a \approx 10^\circ$. Crystals are pleochroic with X colourless, Y and Z
117 light green-yellow; $X < Y \approx Z$. The Gladstone–Dale compatibility, $1 - (K_p/K_C)$, (Mandarino 2007)
118 is -0.009 (superior) based on the empirical formula (using Li, Na, and K based on the structure
119 refinement) using $k(\text{UO}_3) = 0.118$, as provided by Mandarino (1976).

120

121

RAMAN SPECTROSCOPY

122

Raman spectroscopy was conducted on a Horiba XploRA PLUS using a 532 nm diode
123 laser, 50 μm slit, 2400 gr/mm diffraction grating, and a 100 \times (0.9 NA) objective. The spectrum,
124 recorded from 4000 to 100 cm^{-1} , is shown in Figure 3.

125

Two weak bands with centers at 3570 and 3475 cm^{-1} are assigned to $\nu(\text{OH})$ stretching
126 vibrations. Using the empirically derived equation of Libowitzky (1999) the calculated O...O
127 distances of the corresponding hydrogen bonds are between $\sim 3.0 \text{ \AA}$ and $\sim 2.8 \text{ \AA}$, in reasonable
128 agreement with the hydrogen bond lengths determined from the structure refinement. Several
129 very broad low intensity bands centered at ~ 2600 and $\sim 1800 \text{ cm}^{-1}$ are probably overtones or
130 combination bands. No apparent band related to the $\nu_2(\delta)$ bending vibrations of H_2O , is present at
131 approximately 1600 cm^{-1} , which is not surprising considering the low sensitivity of Raman for
132 the non-symmetrical vibrations.

133

There has been no reliable computational/theoretical research focused on differentiating
134 SO_4 and SO_3OH in Raman spectra; therefore, our assignments of the vibrations connected with
135 the sulfate tetrahedra in seaborgite are tentative. The $\nu_3(\text{SO}_4/\text{SO}_3\text{OH})$ antisymmetric stretching
136 vibrations occur as weak bands at 1203, 1194, 1173, 1139, and 1091 cm^{-1} . Several weak to
137 strong bands at 1045, 1026, 1015, 1002, and 979 cm^{-1} are assignable to the ν_1 symmetric
138 stretching vibrations of SO_4 and SO_3OH groups. The presence of six symmetrically unique SO_4

139 tetrahedra in the seaborgite structure lead to the multiple split bands in this region. The weak
140 band at 917 cm^{-1} is related to the $\nu_3(\text{UO}_2)^{2+}$ antisymmetric stretching vibration, while the band at
141 885 cm^{-1} is assigned to the $\nu(\text{S-OH})$ mode (cf. Plášil et al. 2013). The $\nu_1(\text{UO}_2)^{2+}$ symmetric
142 stretching vibration is present as a very strong band at 850 cm^{-1} . Bartlett and Cooney (1989)
143 provided an empirical relationship to derive the approximate U–O_{Ur} bond lengths from the band
144 position assigned to the UO_2^{2+} stretching vibrations, which gives 1.76 \AA (ν_1) and 1.77 \AA (ν_3), in
145 excellent agreement with the average U1–O_{Ur} bond length from the X-ray data: 1.757 \AA . At least
146 seven overlapping weak bands between 657 and 586 cm^{-1} are attributable to the
147 $\nu_4(\delta)(\text{SO}_4/\text{SO}_3\text{OH})$ bending vibrations, with centers at 657 , 647 , 641 , 634 , 621 , 605 , and 586 cm^{-1} .
148 Those at 479 , 463 , 444 , and 425 cm^{-1} belong to the $\nu_2(\delta)(\text{SO}_4/\text{SO}_3\text{OH})$ bending vibrations. A
149 band at 250 cm^{-1} is attributable to the $\nu_2(\delta)(\text{UO}_2)^{2+}$ bending vibrations and/or possibly to $\nu(\text{U-O}_{eq})$
150 bending modes. The remaining bands arise due to unassigned phonon modes.

151

152

CHEMICAL ANALYSIS

153 Chemical analyses for all elements except Li (8 points on 2 crystals) were performed on a
154 JEOL JXA-8230 electron microprobe using Probe for EPMA software. The analytical conditions
155 used were 10 keV accelerating voltage, 10 nA beam current, and a beam diameter of $10\text{ }\mu\text{m}$. Raw
156 X-ray intensities were corrected for matrix effects with a $\phi\rho(z)$ algorithm (Pouchou and Pichoir
157 1991). Time-dependent intensity corrections were applied to data for Na and K. No other
158 elements were detected by EDS and wavescans at multiple currents and beam sizes showed no N
159 above background. Crystals of seaborgite experienced considerable damage under the electron
160 beam. The amount of Na, and to a lesser extent K, reported in the EPMA are significantly lower

161 than those based on the structure refinement; this is attributed to the failure of the time-dependent
162 intensity corrections to fully account for the volatility of Na and K.

163 Li, Na, and U were measured using Laser Ablation Inductively Coupled Plasma Mass
164 Spectrometry (LA-ICP-MS). The ion signals for Li, Na, and U from 2 crystal aggregates were
165 measured using an Element 2 sector field high resolution inductively coupled plasma mass
166 spectrometer (Thermo Fisher Scientific) in low mass resolution mode coupled with a UP-213
167 (New Wave Research) Nd:YAG deep UV (213 nm) laser ablation system. Prior to the ablation of
168 samples, the Element 2 was tuned using a multi-element solution containing $1 \text{ ng} \cdot \text{g}^{-1}$ of each Li,
169 In, and U to obtain maximum ion sensitivity. The laser ablation analyses involved acquiring
170 background ion signals for 60 seconds with the laser on and shuttered, and this was followed by
171 60 seconds of data acquisition. The laser was operated using a $30 \text{ } \mu\text{m}$ spot size, repetition rate of
172 5 Hz, and 65% power output, which corresponded to a fluence of $\sim 8.4 \text{ J} \cdot \text{cm}^{-2}$. Two areas on two
173 crystals were examined using single spot analyses. The background corrected ion signals (counts
174 per second) obtained for Li, Na, and U are reported as an atomic ratio relative to that recorded for
175 U, which was used to calculate a corresponding wt% oxide value, as absolute abundances could
176 not be determined due to a lack of an appropriate matrix-matched external standard. The
177 analytical value obtained for Na, while higher than that obtained by EPMA, is also significantly
178 lower than that based on the structure refinement, as is the value obtained for Li; the
179 “undermeasurements” are probably due to the fact that we cannot adequately account for the
180 ionization efficiency differences.

181 Because insufficient material is available for a direct determination of H_2O , it has been
182 calculated based upon the structure determination ($\text{U}+\text{S} = 7 \text{ apfu}$, $\text{O} = 27 \text{ apfu}$). Analytical data
183 are given in Table 1. The empirical formula using Na measured via EPMA is

184 $\text{Li}_{0.79}\text{Na}_{5.02}\text{K}_{2.02}(\text{UO}_2)(\text{SO}_4)_5(\text{SO}_3\text{OH})(\text{H}_2\text{O})$, which has a charge deficiency of 1.17 due to
185 undermeasurements of Li, K, and Na. The empirical formula using Na measured via LA-ICP-MS
186 is $\text{Li}_{0.79}\text{Na}_{5.19}\text{K}_{2.02}(\text{UO}_2)(\text{SO}_4)_5(\text{SO}_3\text{OH})(\text{H}_2\text{O})$, which has a charge deficiency of 1.00 due to
187 undermeasurements of Li, K, and Na. The empirical formula using Li, Na, and K based on the
188 structure refinement is $\text{Li}_{1.00}\text{Na}_{5.81}\text{K}_{2.19}(\text{UO}_2)(\text{SO}_4)_5(\text{SO}_3\text{OH})(\text{H}_2\text{O})$. The simplified formula is
189 $\text{LiNa}_5(\text{Na,K})\text{K}_2(\text{UO}_2)(\text{SO}_4)_5(\text{SO}_3\text{OH})(\text{H}_2\text{O})$ and the ideal formula is
190 $\text{LiNa}_6\text{K}_2(\text{UO}_2)(\text{SO}_4)_5(\text{SO}_3\text{OH})(\text{H}_2\text{O})$, which requires Li_2O 1.37, Na_2O 17.08, K_2O 8.65, UO_3
191 26.28, SO_3 44.13, H_2O 2.48, total 100 wt%.

192

193 X-RAY CRYSTALLOGRAPHY AND STRUCTURE DETERMINATION

194 Both powder and single-crystal X-ray studies were carried out using a Rigaku R-Axis
195 Rapid II curved imaging plate microdiffractometer with monochromatized $\text{MoK}\alpha$ radiation. For
196 the powder study, a Gandolfi-like motion on the ϕ and ω axes was used to randomize the sample,
197 which consisted of several crystals. Observed d values and intensities were derived by profile
198 fitting using JADE 2010 software (Materials Data, Inc. Livermore, CA). Data are given in
199 Supplemental¹ Table S1. The observed powder diffraction pattern compares very well with the
200 pattern calculated from the crystal structure (Fig. 4)

201 The relatively small crystal size only allowed structure data to be collected to $40^\circ 2\theta$;
202 consequently, the data to parameter ratio (5.45) was less than optimal. The Rigaku CrystalClear
203 software package was used for processing the structure data, including the application of an
204 empirical absorption correction using the multi-scan method with ABSCOR (Higashi 2001). The
205 structure was solved by the charge-flipping method using SHELXT (Sheldrick 2015a). SHELXL-
206 2016 (Sheldrick 2015b) was used for the refinement of the structure.

207 A cation site with scattering power, coordination, bond lengths, and bond valence
208 appropriate for Li was located. (The presence of Li was independently confirmed by LA-ICP-
209 MS.) Nine cation sites other than S, H, and U were located. Two fully occupied by K (K1 and
210 K2), five fully occupied by Na (Na1 thru Na5), one split Na site (Na6a and Na6b) and one
211 occupied jointly by Na and K (Na/K), which refined to $\text{Na}_{0.62}\text{K}_{0.38}$. All non-hydrogen atoms were
212 successfully refined with anisotropic displacement parameters, but several O sites exhibited
213 strongly oblate and/or prolate ellipsoids. This may indicate some local disorder (or local
214 “flexibility”) in the structure, but splitting of the sites did not appear warranted. At least some of
215 the ellipsoid anisotropy may be due to inadequacies in the empirical absorption correction,
216 although a shape-based absorption correction yielded a higher R_{int} and did not lessen the ellipsoid
217 anisotropies.

218 Difference-Fourier syntheses located all H atom positions associated with the H_2O
219 groups, which were then refined with soft restraints of 0.82(3) Å on the O–H distances and
220 1.30(3) Å on the H–H distances and with the U_{eq} of the OH H atom set to 1.5 times the OH O
221 atom and that for each H_2O H atom set to 1.2 times that of the H_2O O atom. The crystallographic
222 data can be found in the original CIF (as supplementary file¹). Selected bond distances are given
223 in Table 2 and a bond-valence analysis in Table 3.

224

225

DISCUSSION

226 The U site in the structure of seaborgite is surrounded by seven O atom sites forming a
227 squat pentagonal bipyramid. This is a typical coordination for U^{6+} in which the two short apical
228 bonds of the bipyramid constitute the uranyl group (cf. Burns, 2005). The two apical O atoms of
229 the bipyramids (O_{Ur}) form short bonds with the U, and this unit comprises the UO_2^{2+} uranyl

230 group. Five equatorial O atoms (O_{eq}) complete the U coordination. All O_{eq} atoms also participate
231 in SO_4 groups. The UO_7 bipyramid is surrounded by five SO_4 tetrahedra centered by S1($\times 2$), S2,
232 S3, and S4, each of which shares one O_{eq} corner of the UO_7 bipyramid. One additional SO_4
233 tetrahedron (centered by S5) and one SO_3OH tetrahedron (centred by S6) are not linked to the
234 UO_7 bipyramid.

235 The UO_7 bipyramids are linked to one another by pairs of SiO_4 tetrahedra to form a
236 $[(UO_2)_2(SO_4)_8]^{4-}$ uranyl-sulfate cluster, which is topologically identical to the cluster in the
237 structure of bluelizardite, $Na_7(UO_2)(SO_4)_4Cl(H_2O)_2$ (Plášil et al. 2014); the two clusters differ in
238 the relative rotation of 1- and 2-connected tetrahedra only, so they can be transformed one into
239 another without the breaking of chemical bonds (Fig. 4). The Li is in regular tetrahedral
240 coordination, typical for Li. Each of the vertices of the LiO_4 tetrahedron is shared with an SO_4
241 tetrahedron ($2 \times S2O_4$ and $2 \times S5O_4$). Two LiO_4 tetrahedra and two $S2O_4$ tetrahedra form a four-
242 member corner-sharing $(LiO_2)_2(S2O_4)_2$ ring in the $\{100\}$ plane; the $[(UO_2)_2(SO_4)_8]^{4-}$ uranyl-
243 sulfate clusters and the $(LiO_2)_2(S2O_4)_2$ rings link through the $S2O_4$ tetrahedra to form a band
244 lying in the $\{100\}$ plane and extending along $[010]$ (Fig. 5). The $S5O_4$ tetrahedra form links in
245 the $[100]$ direction between LiO_4 tetrahedra in adjacent bands. The UO_7 pentagonal bipyramids,
246 LiO_4 tetrahedra, and SO_4 tetrahedra (centered by S1 through S5) thereby form a thick
247 heteropolyhedral layer parallel to $\{001\}$ (Fig. 6). The $S6O_3OH$ tetrahedron does not participate in
248 this layer linkage.

249 The two K sites (K1 and K2) are both eight coordinated, as is the mixed Na/K site. The
250 Na1, Na2, Na4, and Na5 sites are six coordinated, the Na3 site is seven coordinated and the split
251 Na6 sites (Na6a and Na6b) are each five coordinated. All bond valence sums (Table 7) for these
252 large monovalent cation sites are reasonable. The K1 site is located at the center of channels that

253 run through the center of the heteropolyhedral layer. The other large cation sites K2, NaK, Na1,
254 Na2, Na3, Na4, and Na5, as well as the S6O₃OH tetrahedron and the OW27 H₂O group occupy
255 the space between and around the periphery of the heteropolyhedral layers with bonding between
256 them resulting in a framework (Fig. 7). Among all structures containing U⁶⁺, that of seaborgite is
257 unique.

258 Nevertheless, in spite of the structural uniqueness of seaborgite, it is noteworthy that its
259 structural complexity, $I_{G,\text{total}} = 510.17$ bits/cell (after Krivovichev 2012, 2013, 2014, 2018), falls
260 within the most frequent range of complexities observed for uranyl sulfates, 500 to 600 bits/cell
261 (Gurzhiy and Plášil 2019).

262

263

IMPLICATIONS

264 Seaborgite is the first uranyl mineral that contains structurally essential lithium, although
265 many synthetic inorganic compounds contain both lithium and uranium. Only two synthetic
266 uranyl sulfates contain lithium, and these are exotic nanoscale cage cluster compounds (Qiu et al.
267 2017). In seaborgite, the lithium cations are in tetrahedral coordination with the four oxygen
268 atoms contributed by monodentate sulfate tetrahedra. Whereas the fundamental building blocks
269 consisting of uranyl dimers connected to eight sulfate tetrahedra in seaborgite have been observed
270 in other minerals and synthetic compounds, the presence of the lithium-centered tetrahedra
271 stitches these together with additional sulfate tetrahedra to form highly unique uranyl sulfate
272 layers. Within these layers are infinite rods consisting of lithium and sulfate tetrahedra that are
273 made possible by the small size of the lithium cation. The large hydrated radius of lithium that
274 consists of two hydration spheres and its high enthalpy of hydration indicate it is unlikely that
275 extended uranyl sulfate units containing lithium polyhedra exist in the aqueous solution from

276 which seaborgite crystallized. Incorporation of lithium tetrahedra in the structure of seaborgite
277 occurred during crystallization caused by evaporation likely close to dryness, and the uncommon
278 coexistence of sufficient uranyl ions and lithium cations in the same natural aqueous solution
279 combined to produce this unusual mineral and its corresponding structure.

280

281

ACKNOWLEDGEMENTS

282 Sergey Krivovichev, an anonymous reviewer and the Technical Editor are thanked for
283 constructive comments, which improved the manuscript. Associate Editor G. Diego Gatta is
284 thanked for shepherding the manuscript through the review process. Funding to the University of
285 Notre Dame was provided by the Chemical Sciences, Geosciences and Biosciences Division,
286 Office of Basic Energy Sciences, Office of Science, U.S. Department of Energy, Grant No. DE-
287 FG02-07ER15880. Funding to JP was provided by the Czech Science Foundation (20-11949S).
288 This study was also funded by the John Jago Trelawney Endowment to the Mineral Sciences
289 Department of the Natural History Museum of Los Angeles County.

290

291

REFERENCES

292 Bartlett, J.R., and Cooney, R.P. (1989) On the determination of uranium-oxygen bond lengths in
293 dioxouranium(VI) compounds by Raman spectroscopy. *Journal of Molecular Structure*, 193,
294 295–300.
295 Burns, P.C. (2005) U^{6+} minerals and inorganic compounds: Insights into an expanded structural
296 hierarchy of crystal structures. *The Canadian Mineralogist*, 43, 1839–1894.

- 297 Chenoweth, W.L. (1993) The Geology and Production History of the Uranium Deposits in the
298 White Canyon Mining District, San Juan County, Utah. Utah Geological Survey
299 Miscellaneous Publication, 93–3.
- 300 Ferraris, G., and Ivaldi, G. (1988) Bond valence vs bond length in O···O hydrogen bonds. Acta
301 Crystallographica, B44, 341–344.
- 302 Gagné, O.C., and Hawthorne, F.C (2015) Comprehensive derivation of bond-valence parameters
303 for ion pairs involving oxygen. Acta Crystallographica, B71, 562–578.
- 304 Gunter, M.E., Bandli, B.R., Bloss, F.D., Evans, S.H., Su, S.C., and Weaver, R. (2004) Results
305 from a McCrone spindle stage short course, a new version of EXCALIBUR, and how to build a
306 spindle stage. The Microscope, 52, 23–39.
- 307 Gurzhiy, V.V., and Plášil, J. (2019) Structural complexity of natural uranyl sulfates. Acta
308 Crystallographica, B75, 39–48.
- 309 Higashi, T. (2001) ABSCOR. Rigaku Corporation, Tokyo.
- 310 Kampf, A.R., Plášil, J., Kasatkin, A.V., Marty, J., and Cejka, J. (2015) Fermiite,
311 $\text{Na}_4(\text{UO}_2)(\text{SO}_4)_3 \cdot 3\text{H}_2\text{O}$ and oppenheimerite, $\text{Na}_2(\text{UO}_2)(\text{SO}_4)_2 \cdot 3\text{H}_2\text{O}$, two new uranyl sulfate
312 minerals from the Blue Lizard mine, San Juan County, Utah, USA. Mineralogical Magazine,
313 79, 1123–1142.
- 314 Krivovichev, S.V. (2012): Topological complexity of crystal structures: quantitative approach.
315 Acta Crystallographica, A68, 393–398.
- 316 Krivovichev, S.V. (2013): Structural complexity of minerals: information storage and processing
317 in the mineral world. Mineralogical Magazine, 77, 275–326.
- 318 Krivovichev, S.V. (2014): Which inorganic structures are the most complex? Angewandte
319 Chemie, International Edition English, 53, 654–661.

- 320 Krivovichev, S.V. (2018): Ladders of information: what contributes to the structural complexity
321 of inorganic crystals. *Zeitschrift für Kristallographie*, 233, 155–161.
- 322 Libowitzky, E. (1999) Correlation of O-H stretching frequencies and O-H···O hydrogen bond
323 lengths in minerals. *Monatshefte für Chemie*, 130, 1047–1059.
- 324 Lussier A.J., Lopez R.A.K., and Hawthorne, F.C. (2016) A revised and expanded structure
325 hierarchy of natural and synthetic hexavalent uranium compounds. *Canadian Mineralogist*,
326 54, 177–283.
- 327 Mandarino, J.A. (1976) The Gladstone-Dale relationship – Part 1: derivation of new constants.
328 *Canadian Mineralogist*, 14, 498–502.
- 329 Mandarino, J.A. (2007) The Gladstone–Dale compatibility of minerals and its use in selecting
330 mineral species for further study. *Canadian Mineralogist*, 45, 1307–1324.
- 331 Plášil, J., Kampf, A.R., Kasatkin, A.V., Marty, J., Škoda, R., Silva, S., and Čejka, J. (2013)
332 Meisserite, $\text{Na}_5(\text{UO}_2)(\text{SO}_4)_3(\text{SO}_3\text{OH})(\text{H}_2\text{O})$, a new uranyl sulfate mineral from the Blue
333 Lizard mine, San Juan County, Utah, USA. *Mineralogical Magazine*, 77, 2975–2988.
- 334 Plášil, J., Kampf, A.R., Kasatkin, A.V., and Marty, J. (2014) Bluelizardite,
335 $\text{Na}_7(\text{UO}_2)(\text{SO}_4)_4\text{Cl}(\text{H}_2\text{O})_2$, a new uranyl sulfate mineral from the Blue Lizard mine, San Juan
336 County, Utah, USA. *Journal of Geosciences*, 59, 145–158.
- 337 Pouchou, J.-L., and Pichoir, F. (1991) Quantitative Analysis of Homogeneous or Stratified
338 Microvolumes Applying the Model “PAP.” Pp. 31–75 in: *Electron Probe Quantitation*.
339 Springer US, Boston, MA.
- 340 Qiu, J., Spano, T.L., Dembowski, M., Kokot, A.M., Szymanowski, J.E.S., and Burns, P.C. (2017)
341 Sulfate-centered sodium-icosahedron-templated uranyl peroxide phosphate cages with uranyl
342 bridged by $\mu\text{-}\eta^1\text{:}\eta^2$ peroxide. *Inorganic Chemistry*, 56, 1874–1880.

343 Sheldrick, G.M. (2015a) SHELXT – Integrated space-group and crystal-structure determination.

344 Acta Crystallographica, A71, 3–8.

345 Sheldrick, G.M. (2015b) Crystal structure refinement with SHELXL. Acta Crystallographica,

346 C71, 3–8.

347

348 **Endnote:**

349 ¹Deposit item AM-20-XXXXX, Supplemental tables and CIF. Deposit items are free to all

350 readers and found on the MSA website, via the specific issue’s Table of Contents (go to

351 http://www.minsocam.org/MSA/AmMin/TOC/2020/Xxx2020_data/Xxx2020_data.html).

352

FIGURE CAPTIONS

- 353
- 354
- 355 Figure 1. Diverging group of seaborgite blades with ferrinatrite. The field of view is 0.68 mm
356 across.
- 357
- 358 Figure 2. Crystal drawing of seaborgite; clinographic projection in non-standard orientation.
- 359
- 360 Figure 3. The Raman spectrum of seaborgite recorded with a 532 nm laser.
- 361
- 362 Figure 4. The observed powder diffraction pattern compared with the pattern simulated from the
363 lines calculated from the crystal structure.
- 364
- 365 Figure 5. The $[(\text{UO}_2)_2(\text{SO}_4)_8]^{4-}$ uranyl sulfate clusters in seaborgite (approx. down [100]) and
366 bluelizardite (down [010]).
- 367
- 368 Figure 6. The band along [010] in seaborgite composed of UO_7 pentagonal bipyramids, LiO_4
369 tetrahedra, and SO_4 tetrahedra (S1 thru S4); the S5 SO_4 tetrahedron, which links the bands in the
370 [100] direction is also shown. The view is down [100] and the unit cell outline is shown as
371 dashed lines.
- 372
- 373 Figure 7. The thick heteropolyhedral layers parallel to [001] in seaborgite viewed along the chain
374 direction [010]. Note that the S5 SO_4 tetrahedron links the bands in the [100] direction. The unit
375 cell outline is shown as dashed lines.

376

377 Figure 8. The crystal structure of seaborgite viewed down [100]. The K1, K2, and Na/K
378 coordinations are shown ball-and-stick style. The unit cell outline is shown as dashed lines.

379

380

381 Table 1. Chemical analytical results for seaborgite.

Constituent	Mean	Range	Stand. Dev.	Standard	Structure
Li ₂ O	1.09 [§]	1.04-1.11	0.03		1.38*
Na ₂ O	14.83 [§]	14.67-15.00	0.23		
Na ₂ O	14.34	12.28-15.80	1.14	albite	16.60*
K ₂ O	8.75	7.95-10.98	0.97	orthoclase	9.50*
UO ₃	26.50	24.08-27.96	1.37	syn. UO ₂	26.50
SO ₃	44.27	42.13-47.57	2.01	anhydrite	44.27
H ₂ O	2.49*				2.49*
Total	97.93 [†] 97.44 [‡]				100.74

382 * based upon the structure refinement.

383 § measured by LA-ICP-MS

384 † using Na measured via EPMA

385 ‡ using Na measured via LA-ICP-MS

386

387 Table 2. Selected bond distances (Å) and angles (°) for seaborgite.
 388

389	Li–O20	1.94(2)	Na5–O2	2.337(10)	U–O25	1.754(8)	
390	Li–O7	1.96(2)	Na5–O21	2.375(11)	U–O26	1.759(8)	
391	Li–O5	1.97(2)	Na5–O20	2.461(10)	U–O12	2.292(9)	
392	Li–O17	2.05(2)	Na5–O18	2.476(10)	U–O16	2.360(9)	
393	<Li–O>	1.98	Na5–O15	2.508(10)	U–O3	2.365(9)	
394			Na5–O13	2.573(10)	U–O4	2.377(8)	
395	Na/K–O6(×2)	2.491(9)	<Na5–O>	2.455	U–O8	2.488(8)	
396	Na/K–O17(×2)	2.740(10)			<U1–O _{Ur} >	1.757	
397	Na/K–O5(×2)	2.881(9)	Na6a–O23	2.284(18)	<U1–O _{eq} >	2.376	
398	Na/K–O7(×2)	3.095(10)	Na6a–O15	2.328(16)			
399	<Na/K–O>	2.802	Na6a–O13	2.341(15)	S1–O1	1.447(9)	
400			Na6a–O22	2.345(19)	S1–O2	1.465(9)	
401	Na1–OW27(×2)	2.345(11)	Na6a–O11	2.55(4)	S1–O3	1.483(9)	
402	Na1–O11(×2)	2.394(8)	<Na6a–O>	2.370	S1–O4	1.495(9)	
403	Na1–O14(×2)	2.534(8)			<S1–O>	1.473	
404	<Na1–O>	2.425	Na6b–O23	2.271(17)			
405			Na6b–O22	2.307(17)	S2–O5	1.458(10)	
406	Na2–O1	2.311(11)	Na6b–O15	2.342(15)	S2–O6	1.459(9)	
407	Na2–O2	2.333(9)	Na6b–O13	2.414(17)	S2–O7	1.461(9)	
408	Na2–O13	2.377(10)	Na6b–O18	2.55(4)	S2–O8	1.502(9)	
409	Na2–O15	2.415(10)	<Na6b–O>	2.377	<S2–O>	1.470	
410	Na2–O25	2.415(10)					
411	Na2–O16	2.768(10)	K1–O1	2.650(9)	S3–O9	1.447(9)	
412	<Na2–O>	2.437	K1–O3	2.799(8)	S3–O10	1.475(8)	
413			K1–O5	2.799(9)	S3–O11	1.476(9)	
414	Na3–O10	2.379(10)	K1–O17	2.809(10)	S3–O12	1.499(9)	
415	Na3–O14	2.412(10)	K1–O2	2.818(9)	<S3–O>	1.474	
416	Na3–OW27	2.434(11)	K1–O26	2.840(9)			
417	Na3–O9	2.502(10)	K1–O8	2.971(9)	S4–O13	1.450(9)	
418	Na3–O22	2.567(10)	K1–O6	2.979(9)	S4–O14	1.452(9)	
419	Na3–O11	2.590(10)	<K1–O>	2.833	S4–O15	1.463(8)	
420	Na3–O23	2.658(11)			S4–O16	1.502(9)	
421	<Na3–O>	2.506	K2–O21	2.755(9)	<S4–O>	1.467	
422			K2–O10	2.764(9)			
423	Na4–O9	2.302(10)	K2–O22	2.765(9)	S5–O17	1.454(10)	
424	Na4–O10	2.313(10)	K2–O9	2.889(9)	S5–O18	1.468(9)	
425	Na4–O6	2.450(10)	K2–O20	2.897(10)	S5–O19	1.470(9)	
426	Na4–O7	2.521(10)	K2–O23	2.897(10)	S5–O20	1.487(9)	
427	Na4–O19	2.760(11)	K2–O19	2.955(9)	<S5–O>	1.470	
428	Na4–O8	2.775(10)	K2–O19	2.960(9)			
429	<Na4–O>	2.520	<K2–O>	2.860	S6–O21	1.411(9)	
430					S6–O22	1.444(9)	
431	<i>Hydrogen bonds</i>				S6–O23	1.458(9)	
432	<i>D–H···A</i>	<i>D–H</i>	<i>H···A</i>	<i>D···A</i>	< <i>DHA</i> >	S6–OH24	1.557(10)
433	OH24–H24···O19	0.82(3)	1.91(5)	2.711(14)	166(15)	<S6–O>	1.468
434	OW27–H27a···O14	0.82(3)	2.18(5)	2.963(13)	159(12)		
435	OW27–H27b···O12	0.82(3)	2.35(8)	2.992(14)	135(11)		

436

437 Table 3. Bond valence analysis for seaborgite. Values are expressed in valence units.*
 438

	Li	K1	K2	Na/K	Na1	Na2	Na3	Na4	Na5	Na6a	Na6b	U	S1	S2	S3	S4	S5	S6	H bonds	sum
O1		0.22				0.23							1.60							2.05
O2		0.14				0.22			0.22				1.53							2.11
O3		0.15										0.51	1.46							2.12
O4												0.50	1.42							1.92
O5	0.24	0.15		0.08 ×2↓										1.55						2.02
O6		0.10		0.22 ×2↓				0.21						1.55						2.08
O7	0.25			0.05 ×2↓				0.14						1.54						1.98
O8		0.10						0.08				0.39	1.39							1.96
O9			0.12				0.15	0.24								1.60				2.11
O10			0.17				0.20	0.23								1.49				2.09
O11					0.19 ×2↓		0.12			0.14 ×½→					1.49					1.87
O12												0.59			1.40				0.13	2.12
O13						0.20			0.12	0.22 ×½→	0.18 ×½→					1.59				2.11
O14					0.14 ×2↓		0.18									1.58			0.14	2.04
O15						0.18			0.14	0.22 ×½→	0.22 ×½→					1.54				2.08
O16						0.08						0.51				1.39				1.98
O17	0.21	0.15		0.12 ×2↓													1.57			2.05
O18									0.16		0.14 ×½→						1.52			1.75
O19			0.10 0.10					0.08									1.51		0.22	2.01
O20	0.25		0.12						0.16								1.45			1.98
O21			0.17						0.20									1.75		2.12
O22			0.16				0.13			0.22 ×½→	0.24 ×½→							1.61		2.13
O23			0.12				0.10			0.24 ×½→	0.26 ×½→						1.55			2.02
OH24																		1.21	-0.22	0.99
O25						0.18						1.85								2.03
O26		0.14										1.83								1.97
OW27					0.21 ×2↓		0.17												-0.13 -0.14	0.11
sum	0.95	1.15	1.06	0.94	1.08	1.09	1.05	0.98	1.00	1.04	1.04	6.18	6.01	6.03	5.98	6.10	6.05	6.12		

439 * Bond valence parameters are from Gagne and Hawthorne (2015). Hydrogen-bond strengths are
 440 based on O–O bond lengths from Ferraris and Ivaldi (1988).

Figure 1

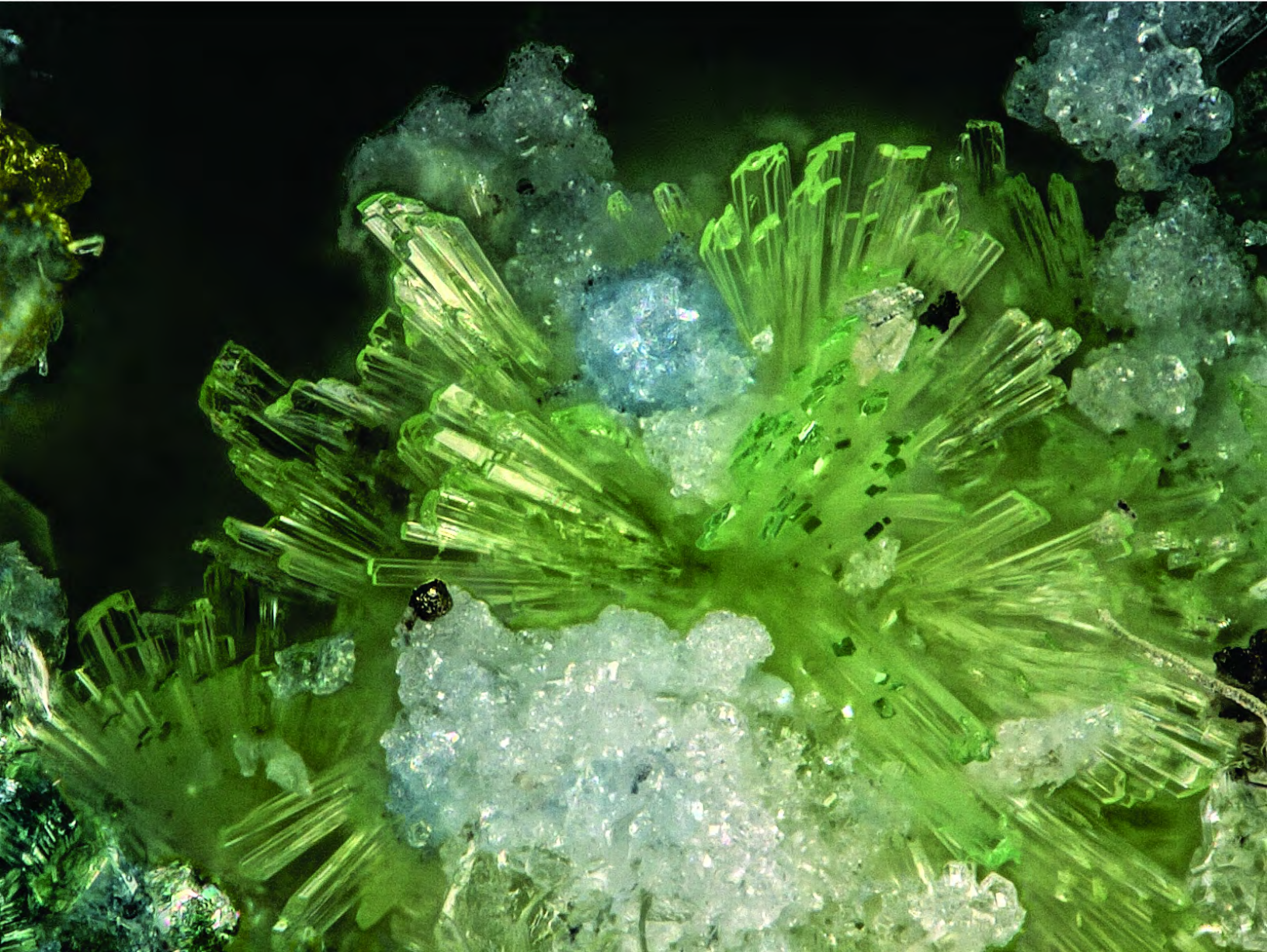


Figure 2

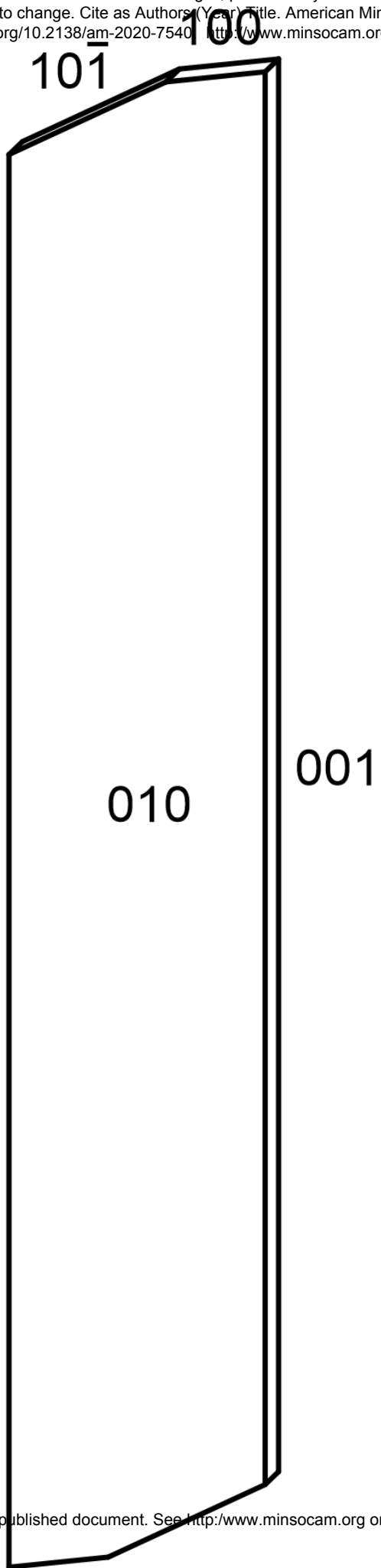


Figure 3

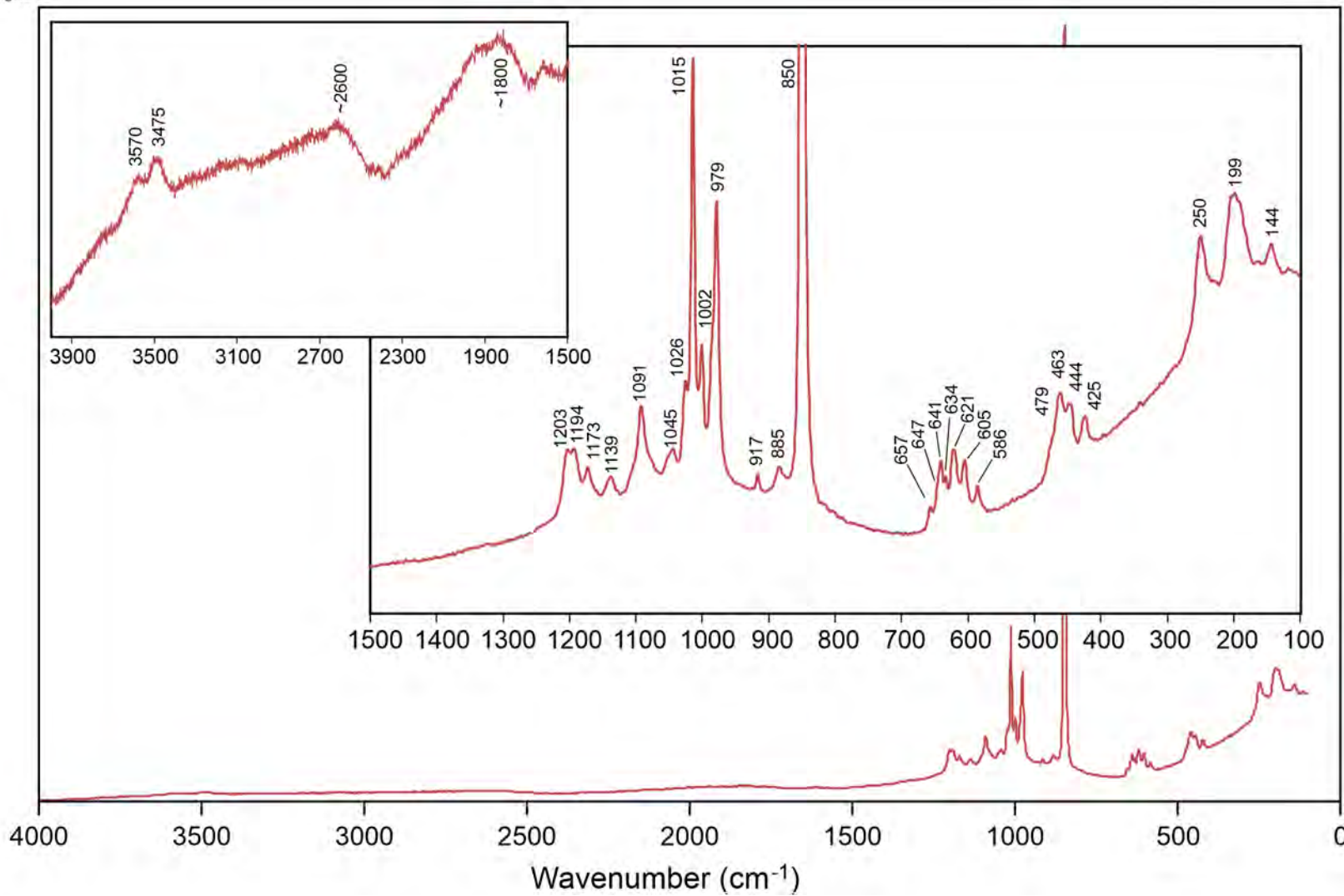


Figure 4

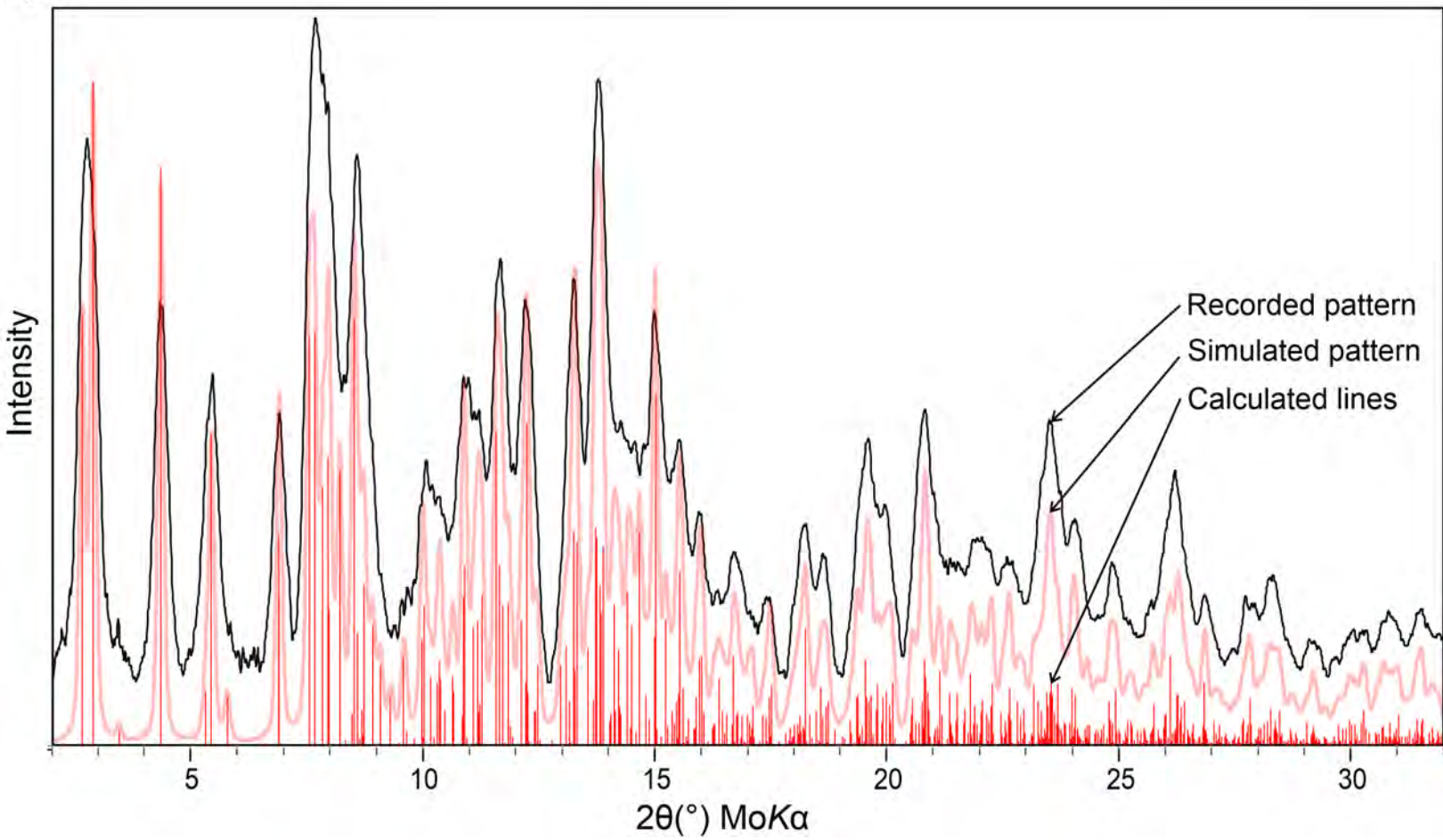


Figure 5

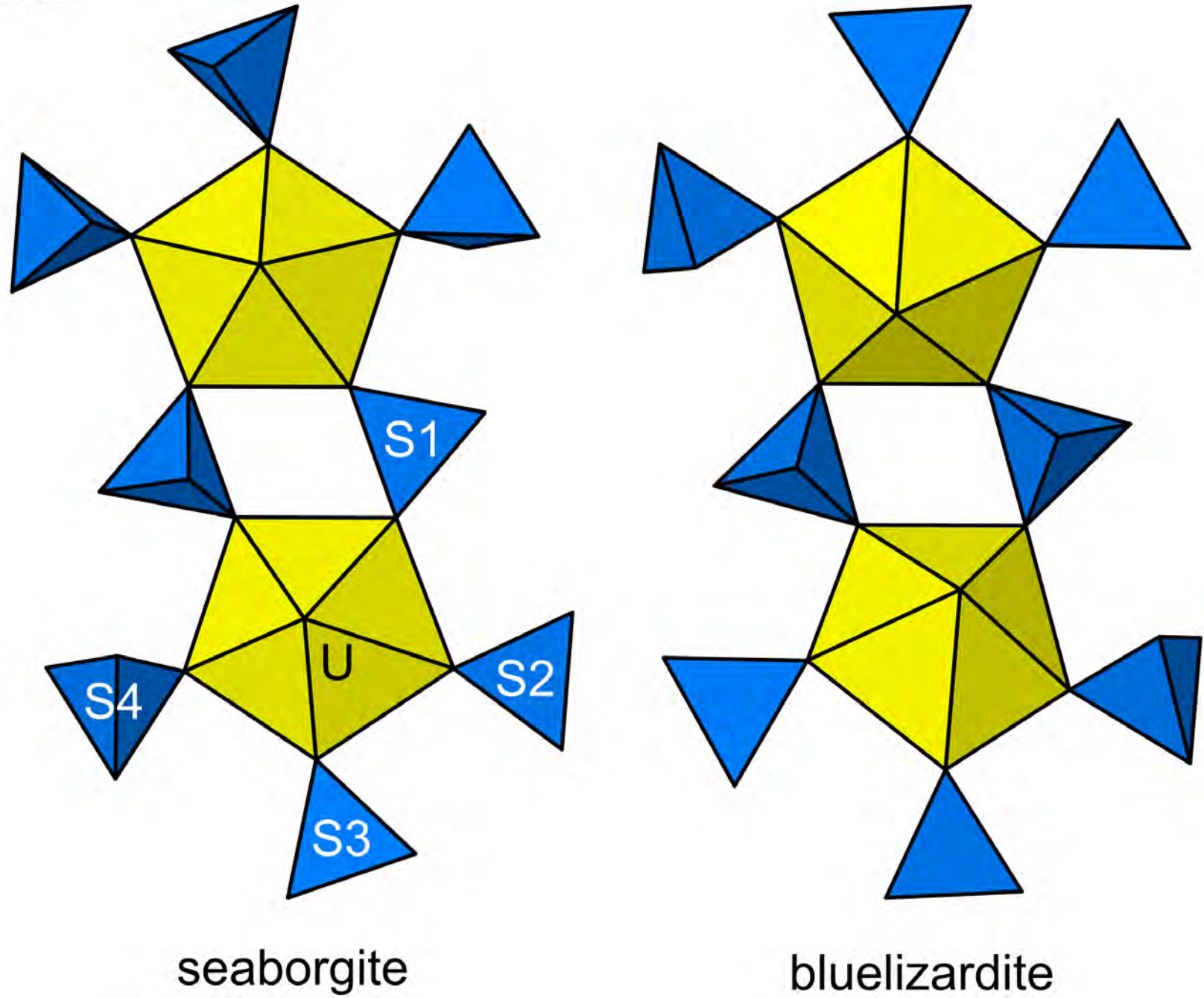


Figure 6

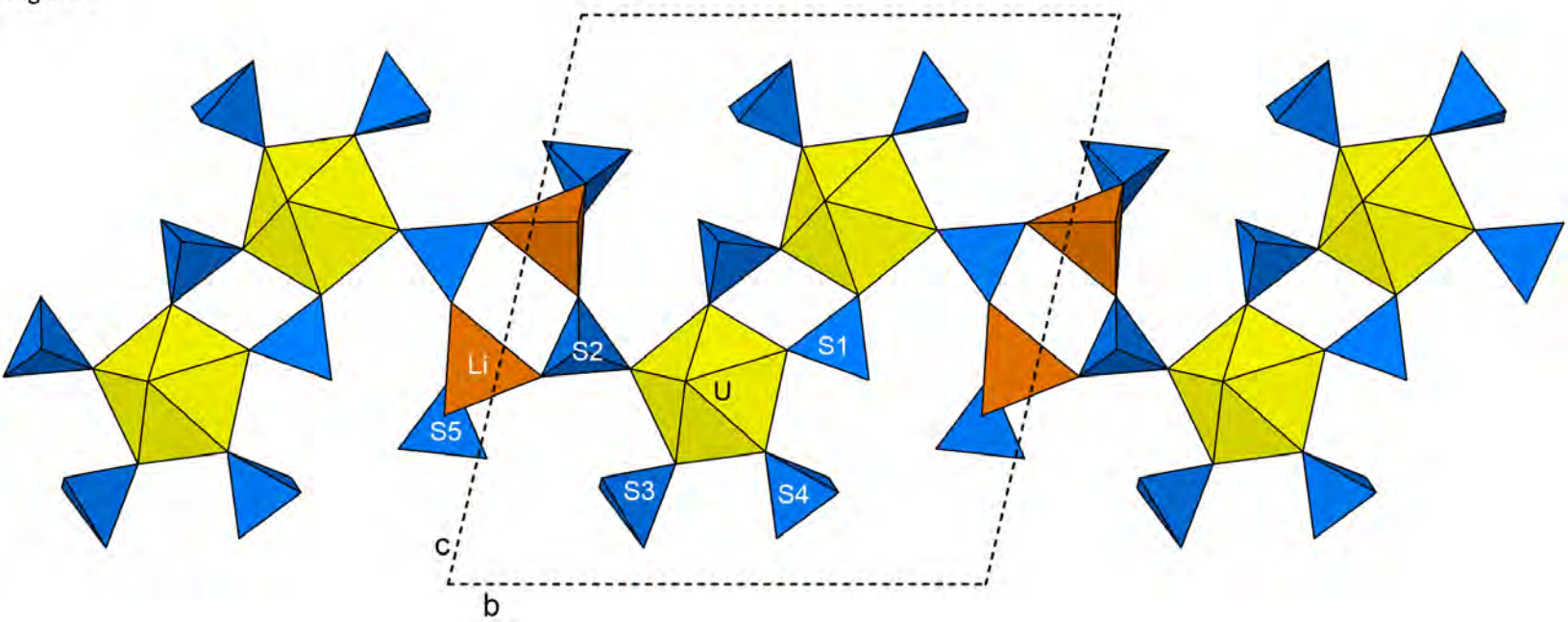


Figure 7

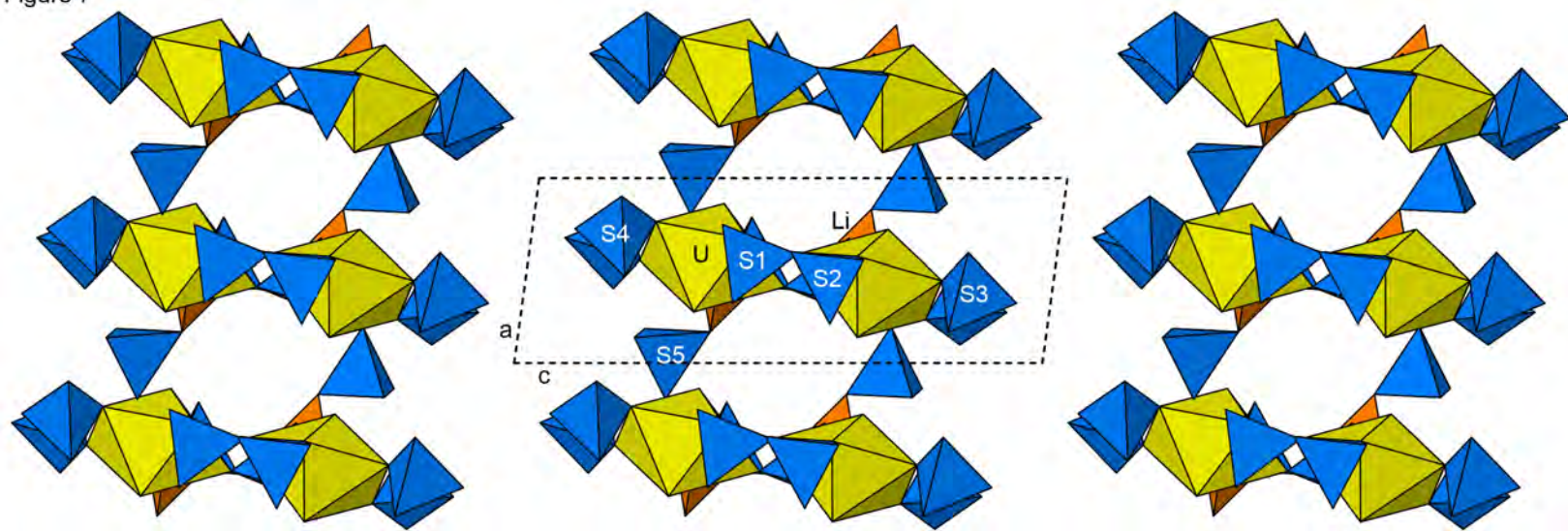


Figure 8

